

Crossover from compact to branched films in electrodeposition with surface diffusion

F. D. A. Aarão Reis*

*Instituto de Física, Universidade Federal Fluminense,
Avenida Litorânea s/n, 24210-340 Niterói, RJ, Brazil*

Dung di Caprio†

*PSL Research University, Chimie ParisTech - CNRS,
Institut de Recherche de Chimie Paris, 75005, Paris, France*

Abdelhafed Taleb‡

Université Pierre et Marie Curie, 4 place Jussieu, 75231, Paris, France

We study a model for thin film electrodeposition in which instability development by preferential adsorption and reduction of cations at surface peaks competes with surface relaxation by diffusion of the adsorbates. The model considers cations moving in a supported electrolyte, adsorption and reduction when they reach the film surface, and consequent production of mobile particles that execute activated surface diffusion, which is represented by a sequence of random hops to neighboring lattice sites with a maximum of G hop attempts ($G \gg 1$), a detachment probability $\epsilon < 1$ per neighboring particle, and a no-desorption condition. Computer simulations show the formation of a compact wetting layer followed by the growth of branched deposits. The maximal thickness z_c of that layer increases with G , but is weakly affected by ϵ . A scaling approach describes the crossover from smooth film growth to unstable growth and predicts $z_c \sim G^\gamma$, with $\gamma = 1/[2(1-\nu)] \approx 0.43$, where $\nu \approx 0.30$ is the inverse of the dynamical exponent of the Villain-Lai-Das Sarma equation that describes the initial roughening. Using previous results for related deposition models, the thickness z_c can be predicted as a function of an activation energy for terrace surface diffusion and the temperature, and the small effects of the parameter ϵ are justified. These predictions are confirmed by the numerical results with good accuracy. We discuss possible applications, with a particular focus on the growth of multifunctional structures with stacking layers of different porosity.

I. INTRODUCTION

Electrodeposition is a relatively low cost technique that allows the production of multifunctional thin films and other nanostructures with various structural, optical, electrical, and magnetic properties [1, 2]. Electrodeposition is strongly affected by the diffusive mass transport of species from the electrolyte to the growing surface, which may lead to morphological instabilities [3–5]. This feature motivated the proposal of several stochastic models, starting from the diffusion-limited aggregation (DLA) model [6–8]. Other models consider mechanisms for controlling the diffusional instability and analyze their effects on the long-time morphology of the electrodeposited films [5, 9–12]. On the other hand, several recent works show that the mass transport of adsorbed atoms or molecules on the film surface also affects its morphology [13–17] and detailed investigations of the first stages of electrodeposition of various materials reveal the microscopic mechanisms of adsorbate diffusion [18–20]. Analytic and simulation models also account for those processes [3, 14, 21–23].

The interplay between the diffusional limitations in solution and the surface relaxation (via adsorbate diffusion)

is important to understand the nucleation and growth stages and may have impact on the production of films and other nanostructures with the desired properties. The production of multifunctional films is possible, for instance, by controlled changes in the film structure and architecture [24]. In many cases, deposited films show different stacking layers with different porosities and thicknesses [25], whose different physical and/or chemical properties ensure multifunctional behavior. For example, regarding photovoltaic applications, a layer with large branches and reduced specific surface area ensures the light harvesting, while a layer with small branches enhances the specific surface and favors loading of large molecules (e. g. dyes). These different functions may correspond to conflicting requirements, thus it is necessary to understand how to control the thickness of different layers and the transitions between them. This transition is governed by parameters such as temperature, concentration, potential [26, 27], substrate properties [28], and deposition method [29].

In this work, we introduce a stochastic model for electrochemical deposition that represents cation diffusion in a supported electrolyte and diffusion of the atoms or molecules adsorbed on the electrode or on the film surface. Using numerical simulations, we show the formation of a compact layer near the electrode (a wetting layer) and the development of a branched morphology after a characteristic crossover time. Since these are typical features that provide multifunctional behavior, our aim is

* reis@if.uff.br

† dung.di-caprio@chimie-paristech.fr

‡ abdelhafed.taleb@upmc.fr

to understand how physico-chemical parameters control the length and time scales involved in that crossover. A scaling approach and some results from related models are used to predict the relation between the crossover time and the model parameter related to the surface diffusion coefficient (which in turn depends on an activation energy and temperature). These predictions are in good agreement with the numerical results.

Images of electrodeposited films of different metals have already shown the formation of compact deposits with relatively smooth surfaces before the development of branched morphology [8, 30–35]. However, those works did not analyze this crossover in detail because their focus were long time growth properties, such as surface instability and anomalous scaling of the roughness. Most theoretical approaches for electrodeposition have the same focus; for instance, in systems with instability control mechanisms, a transition from initial unstable growth to standard kinetic roughening may be observed [10, 11]. Instead, the short time crossover analyzed here occurs in the opposite direction: from initial kinetic roughening dominated by surface diffusion [36, 37] to long time instability development.

The rest of this paper is organized as follows. In Section II, we present the electrodeposition model and the quantities of interest in this work. In Section III, we present simulation results for the film density profiles and for the initial kinetic roughening. In Sec. IV, we analyze the relations with other deposition models with adatom surface diffusion. In Section V, a scaling approach is used to determine the film thickness at the crossover from compact to branched morphology, relations to microscopic parameters are analyzed, and possible applications are discussed. In Section VI, a summary of results and conclusions is presented.

II. MODEL AND BASIC CONCEPTS

A. Model definition

This subsection is intended to the presentation of the stochastic rules of the model. The physical interpretation of the model is discussed in Sec. II B.

The model is defined in a simple cubic lattice with lattice constant a and size La in the x and y directions, with periodic boundary conditions in those directions. The substrate (working electrode) is at the plane $z = 0$ and lattice sites with $z > 0$ initially contain a supported electrolyte.

The deposition occurs by sequential incorporation of aggregated particles, each one occupying one lattice site. These particles may represent atoms or molecules, depending on the electrochemical reaction of interest, which means that the lattice constant a is of the order of some tenths of a nanometer. The incorporation of each particle occurs after a sequence of steps: diffusion of a cation in solution, adsorption on the substrate or on the surface of

the growing deposit, reduction and consequent formation of a mobile particle, and surface diffusion of this particle until it reaches a final aggregation position, where it will be called an aggregated particle. This sequence of steps is described below.

A two-dimensional illustration of the diffusion of the cation in the solution until the adsorption-reduction point is shown in Fig. 1(a). First, a position $(x, y, h_{max} + 45a)$ is chosen for releasing the cation, with random x and y and where h_{max} is the maximal value of z of a previously aggregated particle. This choice describes an approximately uniform distribution of cations at a height which is not very close to the deposit. The cation executes random walks to nearest neighbor (NN) sites in the electrolyte. Its position z cannot exceed $h_{max} + 45a$, i. e. it is reflected at that height. When the cation reaches a site in which at least one NN is an aggregated particle or a substrate site, it is immediately reduced. The product of the electrochemical reaction occupies the same site and is hereafter called a mobile particle. No activation barrier is considered for the processes of cation adsorption and reduction.

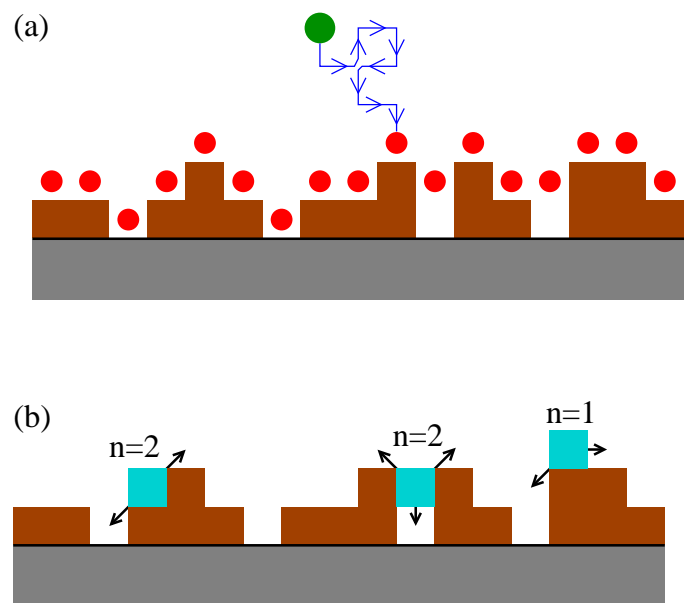


FIG. 1. Two-dimensional representation of the deposition model. (a) The region near the substrate (grey) with some aggregated particles (brown squares) has points available for cation adsorption and reduction indicated by red circles. A cation (green circle) executes a random walk in solution (blue line with arrows) until it reaches one of those points. (b) Possible hops of mobile particles (light blue squares) at three different positions with the corresponding number of NNs indicated.

During the growth of a film, the mobility of an adsorbed species is expected to increase with temperature and to depend on the local surface morphology. The diffusion length of this species will be finite because it will be eventually covered (buried) by other atoms or

molecules. For these reasons, here the mobile particle executes a sequence of hops to neighboring sites, with rules that privilege (but do not oblige) the aggregation at points with high coordination, and the number of hops is constrained to have a maximal value. Moreover, our model assumes that the adsorption states have energy sufficiently small to forbid desorption, even in the cases where large diffusion lengths are considered.

The diffusion of the mobile particle is represented by a sequence of G attempts to hop to neighboring sites, beginning at the point in which that particle was produced. In each attempt, there are two conditions for the hop to be executed:

A) Let n be the number of occupied NN sites of the current position of the mobile particle (occupied sites are those with an aggregated particle or in the substrate) and

$$P_{hop} = \epsilon^{n-1}, \quad (1)$$

with

$$\epsilon = \exp(-E_b/k_B T), \quad (2)$$

where $E_b > 0$ is an activation energy and T is the temperature (consequently $\epsilon < 1$). With probability $1 - P_{hop}$, the hop is not executed; with probability P_{hop} , the second condition is checked.

B) A target site is randomly chosen among the NN and next nearest neighbor (NNN) sites of the current position. The hop is executed if the target site is empty and has at least one NN which is occupied; otherwise, the hop is not executed. This condition rules out desorption of the mobile particle.

After G attempts to hop, the mobile particle becomes an aggregated particle at its final position.

Fig. 1(b) shows the allowed directions for a hop of three particles at different positions of the deposit in a two dimensional representation of the model.

The time τ is defined as the time of aggregation of L^2 particles, i. e. the time for adsorption of one monolayer. The coverage at time t is t/τ , which corresponds to the number of monolayers in the case of a compact deposit. We will assume that τ is constant, which means that the mass of the deposit increases linearly with the time t ; this assumption approximately corresponds to galvanostatic deposition.

Simulations of the model were performed in lattices with $L = 1024$ until the maximal height reached the value $h_{max} = 2000a$. Several values of G were considered, from 10^2 to 5×10^4 . The values of ϵ were between 0.05 and 0.25. For each set of parameters, 9 different realizations were generated. The lattices are very large, thus each realization contains a very large number of different microscopic environments and the average quantities have relatively small fluctuations (except after the development of long branches, but these long time features are not analyzed in this work). Simulations for some model parameters were performed in lattices with $L = 1536$ for checking for finite-size effects, but maximal heights had to be smaller due to computational limitations.

B. Interpretation of model parameters

The diffusive motion of cations in solution is expected in a supported electrolyte, since the addition of a high concentration of inert ions significantly increases the conductivity, reducing the electric field and suppressing migration of the electroactive ions; for details, see Ref. [38]. At long deposition times, cation migration due to the electric field is expected to affect the film features, as discussed in Sec. VD, but these effects are not considered in the present model.

For any set of model parameters, the formation of the mobile particle when the cation has an occupied NN means that the sticking coefficient for the cation is 1, which corresponds to the absence of activation barriers to go from solution to an adsorption state. Moreover, the cation reduction at the point of adsorption means that the rate of the electrochemical reaction is very large, which is possible if the cathodic potential is sufficiently negative.

Now consider the case $G = 0$. The product of the electrochemical reaction is not mobile in this case, i. e. it permanently aggregates at the position where the cation was reduced. Thus, the model becomes equivalent to the diffusion-limited aggregation (DLA) of Witten and Sander [6], which leads to the formation of highly branched fractal deposits; see e. g. Ref. [7] for the case of growth on a surface. For small G , we also expect to obtain film features similar to those of DLA.

Now consider the growth of a real film in which the adsorbed species is mobile. We expect that this species has a local diffusion coefficient \mathcal{D} which increases with temperature and which depends on the local surface morphology; typically, as the number of neighbors increase, the local value of \mathcal{D} decreases. In a film terrace, the diffusion coefficient is expected to have its maximal possible value Da^2 , where D has an Arrhenius form

$$D = h_0 \exp(-E_s/k_B T), \quad (3)$$

where E_s is a terrace activation energy and h_0 is a hopping frequency. On the other hand, the diffusion process will take place in a finite time because the mobile species will be eventually covered (buried) by other atoms or molecules. This time decreases as the deposition rate F increases, with F defined as the number of reduced cations per substrate site per unit time.

Our model is consistent with these features, although it simplifies the dynamics of adsorbed particles. The mobile particle in a film terrace or in the substrate ($n = 1$) executes G hops, i. e. the surface diffusion always takes place in a finite time. Moreover, if the mobile particle has more than one neighbor ($n > 1$), then the probability P_{hop} [Eq. (1)] represents the reduction in the local value of \mathcal{D} in comparison with the terrace value D .

For the above reasons, we also expect that G increases with D and decreases with F . The discussion on the relation between G and the ratio D/F is postponed to Sec. IV because it will be motivated by the numerical results

and requires the presentation of previous results for other deposition models [39, 40]. However, we anticipate that G is related to D/F by a power law, thus Eq. (3) implies that G depends on the temperature in an Arrhenius form.

Also note that the dependence of P_{hop} on T [Eqs. (1) and (2)] is the same of the Clarke-Vvedensky (CV) model [40, 41] of thin film deposition, in which the bond energy E_b per NN describes the effect of the local surface morphology. The present model and the CV model privilege the aggregation at points with high coordination because P_{hop} is very small at those points.

Similarly to many other thin film growth models [41, 42], our model assumes that the adsorbed states have energy which is sufficiently small compared to that in solution, thus desorption is forbidden. This occurs even in the cases where small surface diffusion barriers (and large diffusion lengths) are considered.

Finally, we recall that the use of limited mobility models (such as the model proposed here) instead of collective diffusion models (e. g. CV model) is essential for the simulation of large deposits in a broad range of parameters; see e. g. Ref. [39].

C. Definition of basic quantities

The density ρ was calculated at each level $z > 0$ for several times. It is given by the ratio of the number of aggregated particles at that level and the horizontal cross-sectional area L^2 . The set of deposited particles with position (x, y) will be called a column of the film.

Since the deposit has overhangs and pores, the height of a given column, $h(x, y)$, is defined as the largest position z of a particle at that column. The set $\{h(x, y)\}$ defines the outer surface of the deposit.

The local roughness in a square box of lateral size r at time t is defined as

$$w(r, t) \equiv \overline{\langle (h - \bar{h})^2 \rangle}^{1/2}, \quad (4)$$

where the overbars denote a spatial average in each box position (root-mean square height fluctuation inside the square box at a given position) and the angular brackets denote a configurational average over all positions of the box (which glides parallel to the substrate) and over different configurations of the deposit at time t .

The autocorrelation function [43, 44] is defined as

$$\Gamma(s, t) \equiv \frac{\left\langle \left[\tilde{h}(\vec{r}_0 + \vec{s}, t) \tilde{h}(\vec{r}_0, t) \right]^2 \right\rangle}{W^2}, \quad s \equiv |\vec{s}|, \quad \tilde{h} \equiv h - \frac{\bar{h}}{\kappa}, \quad (5)$$

where \bar{h} is the global average height of the deposit at time t and W^2 is the global square roughness [defined as in Eq. (4) for $r = L$]. The configurational average in Eq. (5) is taken over different initial positions \vec{r}_0 , different orientations of \vec{s} (directions x and y), and different deposits. Note that $\Gamma(0, t) = 1$ at any time t .

The best method to estimate the lateral correlation length from the autocorrelation function depends on details of the interface morphology [43, 44]. In surfaces with some patterned structure (e. g. mounds), Γ oscillates from positive to negative values as s increases, at fixed time; in these cases, the correlation length $\xi(t)$ may be defined as the first zero of $\Gamma(s, t)$. In surfaces with no pattern, $\Gamma(s, t)$ may oscillate with s before crossing the value $\Gamma = 0$, so that a more suitable definition of a correlation length is [45]

$$\Gamma(\xi, t) = k, \quad (6)$$

with some constant $0 < k < 1$. In this work, we calculate ξ using Eq. (6) in forms consistent with both approaches: $k = 0$ (first zero of Γ) and $k = 0.1$.

D. Kinetic roughening

In systems with normal roughening, the expected scaling of the local roughness in large substrates is [42, 46]

$$w(r, t) = r^\alpha f\left(\frac{r}{\xi}\right), \quad (7)$$

where α is the roughness exponent and f is a scaling function. For $x \equiv r/\xi \ll 1$ (small box sizes), $f(x)$ is constant and we obtain

$$w \sim r^\alpha. \quad (8)$$

This means that a single curve with slope α is observed in $\log w \times \log r$ plots for different times. For large r , those curves split because the saturation value of w (the global roughness) depends on time. The correlation length is expected to scale as

$$\xi \sim t^\nu, \quad (9)$$

where ν is the inverse of the dynamical exponent, which determines the rate of lateral propagation of height fluctuations. Equation (9) is also the scaling of the correlation length ξ_1 defined in Eq. (6).

In systems with intrinsic anomalous roughening [47], the local roughness scales as

$$w(r, t) = r^{\alpha_{loc}} t^\kappa g\left(\frac{r}{\xi}\right), \quad (10)$$

where α_{loc} is the local roughness exponent, the exponent $\kappa > 0$ represents the degree of anomaly of the system, and the scaling function $g(x)$ is also constant for $x \ll 1$. The curves $\log w \times \log r$ at different times now split for small r . The exponent κ is usually called local growth exponent (β_{loc}) in experimental works [32, 48].

When the roughening is dominated by surface diffusion of the adsorbed species, the evolution of the film surface in the hydrodynamic limit (large distances, long times)

is expected to be described by the Villain-Lai-Das Sarma (VLDS) [36, 37] equation:

$$\frac{\partial H}{\partial t} = -\nu_4 \nabla^4 H + \lambda_4 \nabla^2 (\nabla H)^2 + \eta(\vec{r}, t), \quad (11)$$

where $H(\vec{r}, t)$ is a coarse-grained height variable, ν_4 and λ_4 are constants, and η is a Gaussian white noise.

In VLDS growth in two-dimensional substrates, the best estimates of scaling exponents are obtained from simulations of the conserved restricted solid-on-solid models [49, 50], and are very close to one-loop renormalization values [51]: $\alpha \approx 0.67$, $\nu \approx 0.30$, and $\beta \approx 0.20$.

III. SIMULATION RESULTS

A. Basic features of the deposits

In Figs. 2a and 2b, we show films grown with $G = 2 \times 10^3$ and $G = 5 \times 10^4$, respectively, both with $\epsilon = 0.1$.

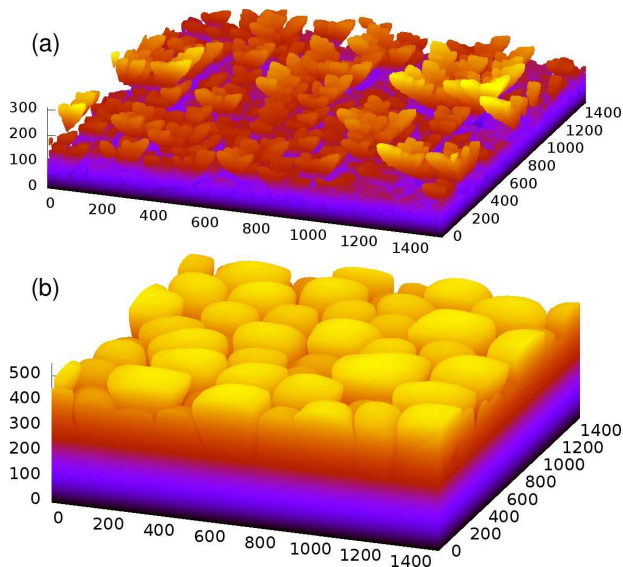


FIG. 2. Deposits grown for (a) $G = 2000$ and (b) $G = 50000$, both with $\epsilon = 0.1$, on a 1536×1536 substrate with periodic boundary conditions in horizontal directions.

For $G = 2 \times 10^3$, a thin wetting layer is formed at short times [darkest colors in Fig. 2(a)]. When some hills and valleys appear at the film surface, the diffusive cation flux leads to preferential growth at those hills. This leads to growth of rounded mounds and eventual formation of overhangs; this is the case of bumps separated by narrow gaps at $z \approx 100$ and below in Fig. 2(a). When high branches are formed [lightest colors in Fig. 2(a)], they reduce all diffusing cations and the mobile particles cannot reach the wetting layer. Thus, the thickness of the wetting layer remains approximately constant while the highest branches continue to grow.

For $G = 5 \times 10^4$, the film is compact until a thickness $h \approx 200a$ is reached, as shown in Fig. 2(b) (darkest

layers). It also has a relatively smooth surface in these conditions. The instability is also developed when thick branches separated by narrow gaps begin to grow [lightest colors in Fig. 2(b)]; their sizes are much larger than those in Fig. 2(a). Again, the wetting layer stops growing when the branches appear because the mobile particles aggregate before reaching that layer.

B. Density profile and crossover thickness

Figs. 3a,b show the density profiles of films deposited with $G = 10^4$ and two values of ϵ and Figs. 3c,d show the density profiles of films deposited with $G = 5 \times 10^4$ and the same values of ϵ . The compact wetting layers correspond to $\rho \approx 1$ near the electrode. At larger heights, $\rho(z) < 1$ indicates that the film is porous; the illustrations in Fig. 2 suggest that most pores are open, but formation of isolated closed pores is also possible.

For $G = 10^4$ (Figs. 3a,b) at short times ($t/\tau \lesssim 100$), the wetting layer is formed and a narrow region with large density gradient is observed above that layer, which corresponds to a rough film surface. As time increases, the wetting layer remains with approximately the same thickness: $h \approx 70a$ for $\epsilon = 0.05$, $h \approx 80a$ for $\epsilon = 0.1$; above that region, a plateau with $\rho \approx 0.6$ is formed for $\epsilon = 0.1$ (from $h \approx 100a$ to $h \approx 350a$). This feature is not observed for $\epsilon = 0.05$ until the maximum times simulated here. A region with large density gradient is then observed, which corresponds to the nucleation and growth of branches above the compact layer. At long times, the density for large z continuously decreases, with a continuous increase in the average film height.

Figs. 3c,d show the density profiles of films deposited with $G = 5 \times 10^4$ and two values of ϵ . The wetting layer is much thicker than that for $G = 10^4$, but the effect of ϵ on its thickness is also small. The density plateau formed above that layer depends on ϵ : $\rho \approx 0.9$ for $\epsilon = 0.05$ [Fig. 3(c)], $\rho \approx 0.8$ for $\epsilon = 0.1$ [Fig. 3(d)]. It corresponds to the thick initial branches separated by narrow gaps, as shown in [Fig. 2(b)]. For $\epsilon = 0.05$, the continuous decrease of the density for large z is observed; for $\epsilon = 0.1$, the plateau with $\rho \approx 0.8$ grows until the maximal simulated times.

The long time density profiles clearly show the crossover from a compact film ($\rho \approx 1$) near the electrode to a film with large density gradient. The region with large gradient may end at a density plateau, which is followed by another region with large density gradient. In all cases, the first of those regions corresponds to the onset of unstable growth, in which branches begin to grow from the protuberances of the surface. The thickness of these branches increases with G , as illustrated in Figs. 2(a) and 2(b).

For a given set of parameters, we define a crossover thickness z_c as the position z in which the density measured at long times is $\rho_c = 0.99$. Figure 4(a) shows z_c as a function of G for three values of ϵ . The effect of ϵ is small, but a significant variation with G is observed.

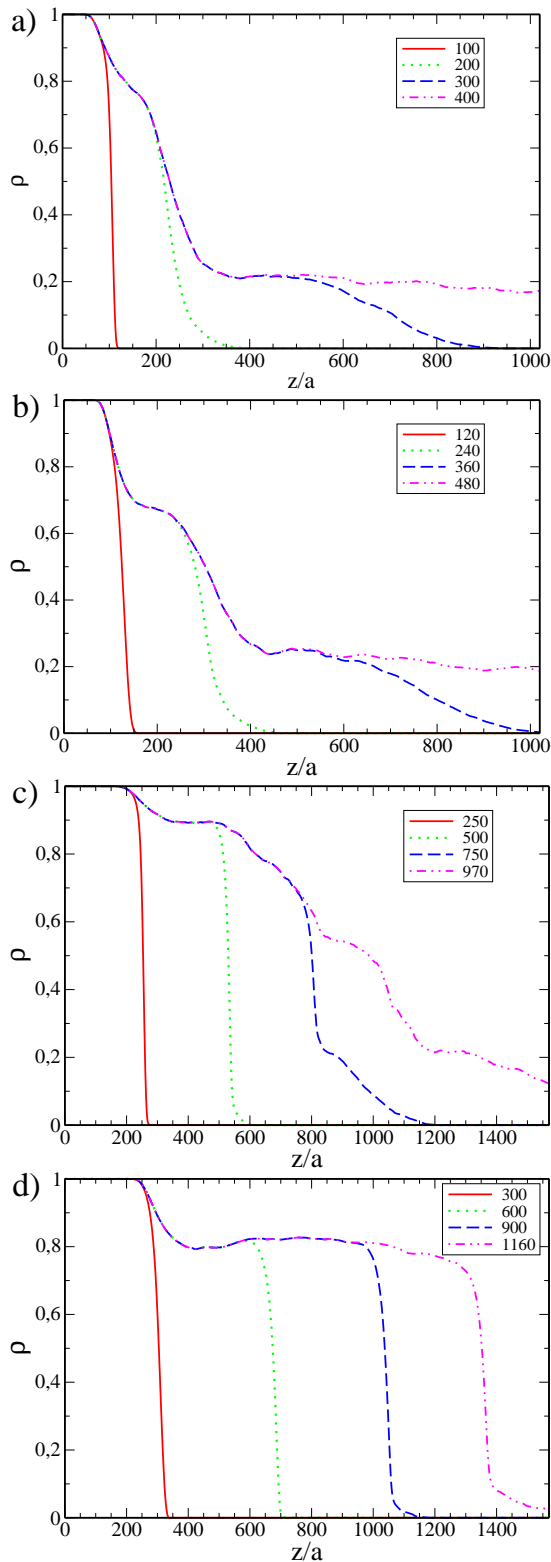


FIG. 3. Density profiles of the films grown with: (a) $G = 10^4$, $\epsilon = 0.05$; (b) $G = 10^4$, $\epsilon = 0.1$; (c) $G = 5 \times 10^4$, $\epsilon = 0.05$; (d) $G = 5 \times 10^4$, $\epsilon = 0.1$. In each plot, the reduced times t/τ (number of aggregated particles per substrate site) are indicated.

The fits in Figure 4(a) for each value of ϵ give

$$\frac{z_c}{a} \sim G^\gamma \quad (12)$$

for large G , with γ between 0.72 and 0.75.

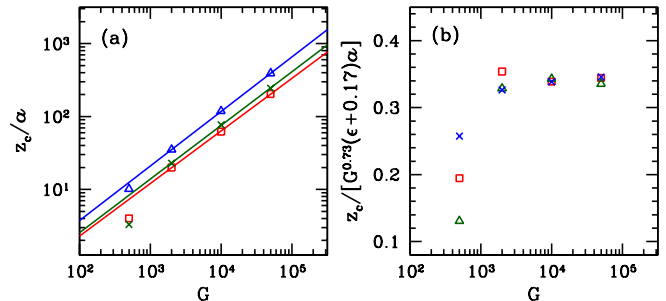


FIG. 4. (a) Crossover height as a function of the parameter G for $\epsilon = 0.05$ (red squares), $\epsilon = 0.1$ (green crosses), and $\epsilon = 0.25$ (blue triangles). Lines are least squares fits of each data set. (b) Scaled crossover height as a function of G for the same values of ϵ .

In order to account for the effect of G and ϵ , Fig. 4(b) shows a scaled crossover thickness as a function of G . It considers $\gamma = 0.73$, which is the exponent that provides the best data collapse for large G and a correction factor depending on ϵ . The relation that follows from this scaling plot for large G is

$$\frac{z_c}{a} \approx 0.34G^\gamma (\epsilon + 0.17). \quad (13)$$

C. Local roughness

In Figs. 5a and 5b, we show the local roughness as a function of box size at several times, for $(G = 5 \times 10^4, \epsilon = 0.1)$ and $(G = 2 \times 10^3, \epsilon = 0.05)$, respectively.

For $G = 5 \times 10^4$ and $t/\tau \leq 100$, we obtain $w/a < 1$ [Fig. 5(a)], which means that the film surface is almost flat, even after deposition of several layers. The scaling of w with r for intermediate times ($t/\tau = 150$ and 200 in Fig. 5(a)) is consistent with normal scaling. The slope for small r is near 0.67, which is the roughness exponent of the VLDS class.

For longer times ($t/\tau \geq 250$), the splitting of the curves for small r is typical of anomalous scaling. However, for a fixed small r , the roughness increases faster than a power law, thus the exponent κ [Eq. (10)] cannot be estimated. This anomaly is only a signature of the onset of unstable growth.

For $G = 2 \times 10^3$, the local roughness shows the typical features of anomalous scaling at short times [Fig. 5(b)]. Again, this behavior is not representative of a true anomalous scaling, but a consequence of the rapid growth of branches separated by deep gaps. At $t/\tau = 50$,

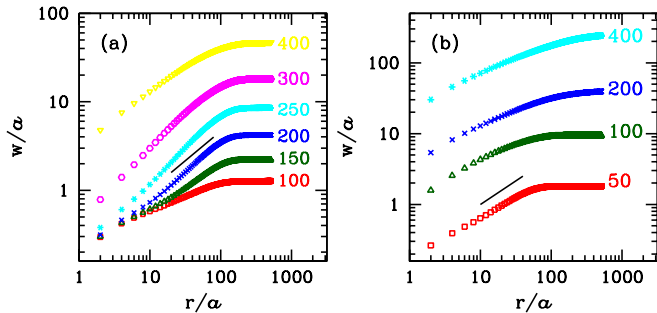


FIG. 5. Local roughness as a function of box size for the times t/τ indicated in the plots, with: (a) $G = 5 \times 10^4$, $\epsilon = 0.10$; (b) $G = 2 \times 10^3$, $\epsilon = 0.05$. The black lines in both plots have slope $2/3$ ($\approx \alpha_{VLDS}$).

the slope of the $\log w \times \log r$ plot is also near the VLDS value 0.67.

D. Correlation length

For small values of G (e. g. $G = 100$), the autocorrelation function Γ has only a shallow minimum for short times, and oscillations disappear at $t/\tau \sim 50$ and longer. This occurs because the instability develops at short times.

For $G = 5 \times 10^4$ and $\epsilon = 0.05$, the autocorrelation function is shown in Fig. 6(a). As time increases, the first minimum of Γ is enhanced (i. e. becomes deeper), which indicates a rapid growth of the protuberant parts of the film. For $t/\tau > 200$, the depth of the minimum is reduced, which indicates that a characteristic length of height fluctuations does not exist in this regime.

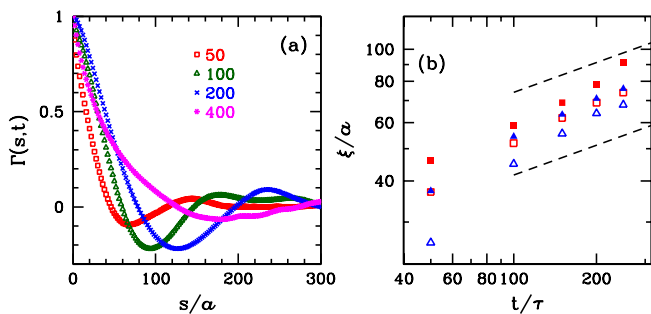


FIG. 6. (a) Autocorrelation function as a function of the horizontal distance s/a at times t/τ indicated in the plot, for $G = 5 \times 10^4$ and $\epsilon = 0.05$. (b) Correlation length as a function of time for ($G = 5 \times 10^4, \epsilon = 0.05$) (squares) ($G = 5 \times 10^4, \epsilon = 0.1$) (triangles), calculated with $k = 0$ (filled symbols) and $k = 0.1$ (empty symbols). The black dashed lines have slope 0.3 ($\approx \nu_{VLDS}$).

The time evolution of the correlation length ξ for ($G = 5 \times 10^4$, $\epsilon = 0.05$) and ($G = 5 \times 10^4$, $\epsilon = 0.1$) is shown in Fig. 6(b), considering Eq. (6) with $k = 0$ and $k = 0.1$. The plotted data is restricted to times $t/\tau \leq 250$, in which there is no evidence of unstable growth. Each data set shows a different evolution and the restricted time range does not allow a reliable extrapolation. However, the average trend of those data is consistent with the exponent $\nu \approx 0.30$ of the VLDS class, as shown in Fig. 6(b).

IV. RELATION WITH OTHER MODELS OF COMPACT FILM GROWTH

The simulation results in Secs. III C and III D suggest that the roughening at short times has VLDS scaling. For this reason, here we analyze the relations with similar models with the same scaling.

The particle diffusion of our model is similar to that of a model introduced in Ref. [39], which is hereafter called lateral aggregation of diffusing particles (LADP). In the LADP, each particle is released above the deposit at a randomly chosen position (x, y) and follows a vertical trajectory until reaching the top of the column of the deposit. The particle subsequently executes random hops to the top of NN columns and permanently aggregates when it has a lateral NN or after executing G hops. Reference [39] also showed that the LADP has VLDS roughening.

There are some differences between our electrodeposition model and the LADP: here we consider a diffusive motion of the cations in solution (instead of the collimated flux of LADP); the hops of mobile particles are allowed to any spatial direction, which may lead to overhang formation (while LADP films are compact); the particle may move if it has two or more occupied NNs (while the LADP corresponds to $\epsilon = 0$). However, these differences are not important at short times, in which the electrodeposition model produces almost compact deposits with small surface roughness, consequently with no significant protuberance. Moreover, the parameter $\epsilon > 0$ has weak effects on the morphology of the compact deposits; the main parameter affecting the surface morphology is G , which has the same role as in the LADP. For the above reasons, the compact film morphology at short times in our electrodeposition model is expected to be similar to that in the LADP. This sets a connection between those models and provides additional evidence for the VLDS scaling of our electrodeposition model at short times.

The scaling of the correlation length of the LADP is of particular importance here [39]:

$$\xi \sim AG^{1/2} \left(\frac{t}{\tau} \right)^\nu a, \quad (14)$$

with $\nu \approx 0.3$ and $A \approx 0.5$. In the electrodeposition model, the amplitude A has a reduction by a factor ~ 8 ,

which is probably due to the frequent rejection of hop attempts (the parameter G in LADP refers only to hops that can be executed).

The LADP was designed for producing deposits with the same morphology of those of the CV model, which was introduced in Ref. [40]. The CV model describes collective adatom diffusion during the deposition and is frequently used to describe molecular beam epitaxy [41]; however, applications to other deposition processes were already proposed [22, 52]. The atomic flux in the CV model is also collimated, with a flux F defined as the number of incident atoms per site per unit time. The solid-on-solid condition is assumed. In one time unit, each surface atom executes an average of $D\epsilon^{n-1}$ hops to NN columns, where D is the terrace diffusion coefficient given in Eq. (3) and ϵ is defined as in Eq. (2). The main parameter to determine the surface features in the CV model is the dimensionless ratio

$$R \equiv \frac{D}{F} = \frac{h_0}{F} \exp\left(-\frac{E_s}{k_B T}\right). \quad (15)$$

When $\epsilon = 0$ (i. e. irreversible lateral aggregation), Ref. [39] showed that the CV model produces deposits with the same roughness of the LADP model with

$$G \sim R^{2\nu}. \quad (16)$$

Recently, Ref. [53] showed that ϵ has a very small effect on the surface features of CV deposits for $0 \leq \epsilon \leq 0.25$. Thus, the LADP also produces film morphology similar to that of the CV model for $\epsilon > 0$ if their parameters are related by Eq. (16).

The above discussion leads to a connection between our electrodeposition model at short times and the CV model. The mobile particle diffusion of our model may be interpreted as an approximation of a collective particle diffusion process. Equations (15) and (16) show that G increases with the diffusion coefficient D and decreases with the deposition rate F , as discussed in Sec. II B:

$$G \sim \left(\frac{h_0}{F}\right)^{2\nu} \exp\left(-\frac{2\nu E_s}{k_B T}\right). \quad (17)$$

Equation (17) also confirms the Arrhenius form expected for G , which was anticipated in Sec. II B.

This connection with VLDS models at short times is the basis for explaining the formation of the films with layers of different morphology when the particle flux is diffusive and to describe the effect of physico-chemical parameters on the crossover thickness.

V. THE CROSSOVER FROM COMPACT TO BRANCHED FILMS

A. Scaling approach

Consider the scheme of Fig. 7, in which a large fluctuation (a hill) appears in the film surface. The autocorrelation function oscillates and has a pronounced minimum,

as illustrated in Fig. 6(a), showing that the lateral size of that fluctuation is of the same order of the correlation length ξ of the initial kinetic roughening.

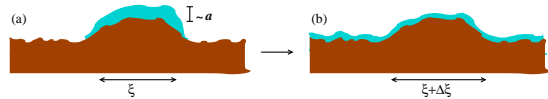


FIG. 7. (a) Schematic view of a deposit (brown) with a protuberant part and a layer of particles (light blue) formed after cation reduction at that protuberance. The correlation length ξ is of the order of the lateral size of the protuberance. (b) Spread of the new layer by diffusion, with increase of the protuberance size.

Most of the cations flowing to the region shown in Fig. 7(a) are reduced in the protuberant part of the surface. Thus, most mobile particles are formed at that region, while a small fraction is formed in the valleys at the hill sides. In a time interval τ , a layer of particles with thickness of order a is formed, thus the velocity of vertical growth of the protuberance is of order

$$v \sim \frac{a}{\tau}. \quad (18)$$

Of course this relation omits a numerical factor (> 1) at the right side due to the preferential reduction at the protuberant part of the surface. However, this factor is of order 1 because we assume an initially small fluctuation.

We expect that the accumulated layer of particles diffuses to the neighboring valleys, as shown in Fig. 7(b). This leads to an increase of the correlation length ξ . The velocity u of lateral flow of material is

$$u \sim \frac{d\xi}{dt} \sim AG^{1/2} \frac{a}{\tau} \left(\frac{t}{\tau}\right)^{\nu-1}, \quad (19)$$

where Eq. (14) was used. The time increase of ξ is always slower than linear because $\nu \leq 1$ (dynamical exponent larger than 1). For this reason, u decreases in time.

If $u > v$, then surface diffusion is able to balance the effect of the preferential adsorption at the protuberance. Thus, normal kinetic roughening is expected, i. e. roughening dominated by the surface diffusion (VLDS scaling). This is expected to occur at short times. On the other hand, if $u < v$, the mass accumulated at the protuberance moves slowly to the neighboring valleys, thus the protuberance height increases. This leads to the unstable growth and is expected at long times. A crossover between the two regimes is expected when those velocities match:

$$v \approx u \quad (t = t_c). \quad (20)$$

Using Eqs. (18), (19), and (20), we obtain

$$\frac{t_c}{\tau} \sim G^\gamma, \quad (21)$$

with

$$\gamma = \frac{1}{2(1-\nu)}. \quad (22)$$

The corresponding crossover thickness is

$$z_c \sim vt_c \sim aG^\gamma. \quad (23)$$

Using the VLDS exponent $\nu \approx 0.30$ [49], we obtain $\gamma \approx 5/7 \approx 0.71$. This agrees with Eq. (12), with an exponent γ in excellent agreement with the simulation results presented in Sec. III B.

This approach is proposed for growth on a flat substrate, but small changes in the crossover thickness z_c are expected if the substrate is rough. For large values of G and substrate roughness of 1-10 lattice units (which typically corresponds to a few nanometers), an initial smoothing process is shown in Ref. [54] for deposition with similar models with collective surface diffusion. The characteristic film thickness necessary for smoothing is $z_s \sim R^{-0.4}(\xi_i/a)^\nu$, where ξ_i is the correlation length of the initial pattern; using Eq. (16), we obtain an estimate $z_s \sim G^{-0.67}\xi_i^\nu$ for our model. For $G \sim 10^3$ and a large initial correlation length $\xi_i/a \sim 10^3$, it gives $z_s < 1$; for larger G , z_s is smaller, thus it is negligible in comparison with z_c . The physical interpretation of this result is that deposition with large G (or R) rapidly fills the valleys of the initial rough pattern, which consequently do not affect the crossover to the branched morphology.

B. Effect of activation energy and temperature

Now we consider the relations with CV models discussed in Sec. IV to determine the crossover thickness z_c as a function of parameters that may be measured experimentally. As a first approximation, we use $h_0 \sim 10^{13}\text{s}^{-1}$ in Eq. (17), which is the value considered when the solid film grows from vapor [41] (although we understand that there are significant difference when the solid surface is in contact with a solution). Using Eq. (13) for very small ϵ and Eq. (22), we obtain

$$\frac{z_c}{a} \sim \frac{10^4}{F^\lambda} \exp\left(-\frac{\lambda E_s}{k_B T}\right), \quad (24)$$

where

$$\lambda = 2\nu\gamma = \frac{\nu}{1-\nu} \approx 0.43. \quad (25)$$

The parameter $\epsilon > 0$ has weak effect in Eq. (24). The amplitude in that equation is a rough estimate due to the uncertainty in h_0 and due to the rejection of hop attempts in the electrodeposition model, which also affects the amplitudes in equations such as (17), as discussed in Sec. IV.

The present model is suitable for a fully supported electrolyte, in which cations in solution move with no bias to

the electrode. Moreover, no effect of additives or other mechanisms that hinder unstable growth is considered. If diffusion bias, additives, etc are present, longer stable regimes are expected, corresponding to larger values of z_c . For this reason, we understand that the present estimate of z_c is a lower bound for the thickness of a compact layer that can be obtained in electrochemical deposition of a given material. This lower bound may be useful in works whose aim is only to obtain branched morphology; these films may be of interest as catalysts or for their particular wetting properties; see, e. g. Ref. [26] for cobalt film electrodeposition.

C. Possible applications

Recent works on electrodeposition of several materials show evidence that surface diffusion is an important mechanism to determine the large scale morphology [13–16, 19–23]. For instance, Xu et al [55] analyzed the kinetic roughening of electrodeposited NiP films and showed exponents very close to those of the VLDS class: $\alpha = 0.70$ and $\beta = 0.16$ (to be compared with $\alpha_{VLDS} \approx 0.67$ and $\beta_{VLDS} \approx 0.20$ [49, 50]). These results give additional support to the model presented in this work.

The formation of a compact layer before the growth of a branched structure is observed in electrochemical deposition of some metals, such as zinc [8], copper [30–34], and silver [35].

In Ref. [30], the thickness of the compact copper layer increases as the overpotential becomes less negative, corresponding to a decrease in the average growth rate. The thicknesses of the compact layers were not reported in that work, but inspection of their images shows an increase by a factor of approximately 2 when the growth rate decreases by a factor of approximately 3, with change of overpotential from -0.35V to -0.15V . This result is qualitatively consistent with the dependence of z_c on F in Eq. (24) with $\lambda < 1$ [Eq. (25)].

The FCC structure of copper differs from the simple cubic lattice used in our simulations, thus our results cannot provide a quantitative description of that material. However, it is interesting to estimate the order of magnitude of quantities that follow from the model application. Electrodeposition of Cu is frequently reported with compact films with thicknesses of a few micrometers, thus we consider the case of $z_c \sim 1\mu\text{m}$ at room temperature. We also consider a lattice constant $a \approx 0.3\text{nm}$ and a current $j \sim 10\text{mA}/\text{cm}^2$, consistently with Refs. [30, 32]; this gives $F \sim 30\text{monolayers}/\text{s}$. Substitution in Eq. (24) gives an exponential factor $\exp[-\lambda E_s/(k_B T)]$ of order 1, which means that $E_s \lesssim 0.05\text{eV}$. This is a very small activation energy, so that diffusion lengths of the deposited atoms can be very large, which highlights the importance of adsorbate diffusion in electrodeposition. However, due to the drastic approximations involved in the derivation of Eq. (24), an accurate estimate of E_s cannot be ob-

tained.

Several technological applications such as photovoltaic, catalysis, sensing, and batteries require highly porous thin layers with limited compact layer, which justifies the present study.

For dye-sensitized solar cell applications, high specific surface of porous materials offers the possibility of high dye loading to sensitize the semiconductor material. Additionally, the branch or the grain size allows the light scattering within the material, which results in extending the path of light, and in turn increases the probability of photons being captured by the sensitizers. However, the increase of film thickness if necessary for the formation of large branches or grains, which causes dye loading reduction and the enhancement of charge recombination processes. The balance between all these conflicting properties requires an accurate tuning of the film thickness [24]. For instance, for porous films made of ZnO aggregates, the optimum thickness to obtain this balance is about $10\mu\text{m}$ [56].

For applications such as batteries [57], sensors [58, 59], or catalysis [60], porous materials provide high active surface areas and shortened pathways for the fast diffusion of reactive species in solution toward the surface. For catalysis and sensors, different optimal thicknesses were reported in the literature, ranging from a few hundred nanometers to a few tens of micrometers, depending on the material, the type of sensor, and the targeted species. However, as the thin film thickness increases, so does the surface area, but the diffusion path length within the material becomes longer, which counterbalances the beneficial effect of the surface area increase. For optimization, a balance between the surface area and the diffusion path length must be found [61, 62].

Other model features may also be considered for some applications. For instance, in metal electrodeposition, Ustarroz et al [18, 19] observed that the initial stages of growth are dominated by coarsening of islands whose building blocks are clusters of a few nanometers, instead of single adatoms. Their sizes may be important for a correct estimate of the smallest lengthscale a and affect the interpretation of activation energies. It is also possible that roughening of a compact film is not described by the VLDS equation; for instance, electrodeposited Ni films of Ref. [16] and Prussian blue films of Ref. [14] have kinetic roughening exponents of the Mullins-Herring equation [63], which is the diffusion-dominated growth model based on Eq. (11) with $\lambda_4 = 0$. In these cases, the scaling exponents of Sec. V A should be changed to consider $\nu = 0.25$ of that class.

D. Relation to other models

Several works have already shown the formation of thin compact films in growth models with diffusion-limited aggregation of the incident species. However, in most cases, one of the following mechanisms was present: large

concentrations of cations in solution, which reduces the thickness of the diffusion layer near the film surface and allows a more uniform flux along the surface of the deposit, or biased diffusion of cations, which also has the asymptotic effect of homogenizing the adsorption rate along the surface.

A simple example was provided in Ref. [9] with DLA of particles that move in a solution with fixed concentration: for large concentrations, dense films with surfaces not very rough were obtained; for intermediate concentrations, porous films resembling ballistic deposits [42] were obtained; for low concentrations, an initial fractal structure is observed, but there is a crossover to growth of a film with finite porosity at long times.

Another example is multiparticle biased DLA (MBDLA) [64, 65], in which cations execute random walks biased toward the electrode ($-z$ direction). In Ref. [10], MBDLA was studied in two dimensions (one-dimensional substrate) including collective diffusion of the adsorbed atoms. The formation of thick branches above a compact film was observed when the surface diffusion coefficient was one order of magnitude smaller than that of diffusion in solution and the bias was low; if those coefficients were equal, then a thick compact film was obtained during all the simulated time. The bias in the particle movement represents the effect of the electric field in solution and always suppresses the unstable growth at long times.

Reference [12] recently presented a continuum electrodeposition model with extended space-charge regions which, for small applied potential, also shows formation of a compact film near the electrode, with thickness increasing with the cation concentration. The phase-field models for electrochemical deposition proposed in Refs. [11, 66] also produce deposits with a compact layer near the (one-dimensional) electrode. In Ref. [11], the main interest was the comparison of the branched morphology with that of experiments on copper [30, 33, 34] instead of the transition discussed in this work.

If a small bias in the motion of cations is included in our model, we also expect that the unstable growth will be asymptotically suppressed. However, the present approach for the compact-to-branched crossover remains valid if this suppression takes place with a sufficiently large film thickness z_s , i. e. if $z_s \ll z_c$.

VI. CONCLUSION

We introduced an electrodeposition model in a simple cubic lattice in which diffusion-limited aggregation of cations in a solution is followed by their reduction and surface diffusion of the adsorbed species, with a maximum of G hops to nearest neighbor sites. Films with overhangs and pores may be formed because adsorption occurs at the first point in which the cation is in contact with the deposit and because diffusion to all directions is allowed, under the condition that all adsorbed particles

remain connected. At short times, compact films with smooth surfaces are formed because diffusion favors aggregation to sites with large number of nearest neighbors. In this regime, the surface roughness and the correlation length scale with exponents close to those of the VLDS class; their scaling is consequently approximated by that of a previously studied model of irreversible lateral aggregation or, equivalently, the Clarke-Vvedensky model of deposition and diffusion without detachment from lateral neighbors. At long times, the films have branches whose widths increase with the number of allowed diffusion hops.

The presence of dense and branched layers in a single film is suitable for applications that require multifunctional behavior. That feature was actually observed in electrodeposited films of several materials. This motivated the study of the relation between the maximal thickness of the compact layer, z_c , and the parameter G , which led to a relation with the activation energy and temperature in an equivalent growth process with collective adatom diffusion. A scaling approach showed that, at short times, the particles formed at surface protuberances can diffuse to distant points, homogenizing the

growth rate along the surface; however, at long times, the lateral size of those protuberances (correlation length) is large, thus the amplitude of surface fluctuations grows in time and branches are subsequently formed. The predictions of that approach were confirmed by numerical simulations.

Whether one seeks multilayers with different features or aims at promoting a layer with specific features, understanding the structure and formation of these layers by electrodeposition is of crucial importance. To this aim, in this paper, we have focused on the onset of the instability related to the transition from dense to ramified layer morphologies. This understanding should allow better control on the thickness of different parts of the layer to adjust to various applications.

ACKNOWLEDGMENT

F.D.A. Aarão Reis acknowledges support from CNPq and FAPERJ (Brazilian agencies).

-
- [1] Y. D. Gamburg and G. Zangari, *Theory and Practice of Metal Electrodeposition*, Springer-Verlag, New York, 2011.
- [2] S. M. Oja, M. Wood, B. Zhang, *Anal. Chem.* **85**, 473-476 (2015).
- [3] R. Aogaki and T. Makino, *J. Electrochem. Soc.* **131**, 40-46 (1984).
- [4] J. Elezgaray, C. Léger, F. Argoul, *J. Electrochem. Soc.* **145**, 2016-2024 (1998).
- [5] M. Haataja, D. J. Srolovitz, *Phys. Rev. Lett.* **89**, 215509:1-4 (2002).
- [6] T. A. Witten Jr., L. M. Sander, *Phys. Rev. Lett.* **47**, 1400-1403 (1981).
- [7] P. Meakin, *Phys. Rev. A* **27**, 2616-2623 (1983).
- [8] F. Argoul, A. Arneodo, G. Grasseau, H. L. Swinney, *Phys. Rev. Lett.* **61**, 2558-2561 (1988).
- [9] M. Uwaha, Y. Saito, *Phys. Rev. A* **40**, 4716-4723 (1989).
- [10] M. Castro, R. Cuerno, A. Sánchez, F. Domínguez-Adame, *Phys. Rev. E* **62**, 161-173 (2000).
- [11] M. Nicoli, M. Castro, R. Cuerno, *J. Stat. Mech.*, P02036:1-15 (2009).
- [12] C. P. Nielsen, H. Bruus, *Phys. Rev. E* **92**, 042302:1-15 (2015).
- [13] Y. Gründer, N. M. Markovic, P. Thompson, C. A. Lucas, *Surf. Sci.* **631**, 123-129 (2015).
- [14] M. F. Alamini, R. C. da Silva, V. C. Zoldan, E. A. Isoppo, U. P. Rodrigues Filho, F. D. A. Aarão Reis, A. N. Klein, A. A. Pasa, *Electrochem. Commun.* **13**, 1455-1458 (2011).
- [15] A. Aryanfar, D. J. Brooks, A. J. Colussi, B. V. Merinov, W. A. Goddard III, M. R. Hoffmann, *Phys. Chem. Chem. Phys.* **17**, 8000-8005 (2015).
- [16] I. S. Brandt, V. C. Zoldan, V. Stenger, C. C. Plá Cid, A. A. Pasa, T. J. Oliveira, F. D. A. Aarão Reis, *J. Appl. Phys.* **118**, 145303 (2015).
- [17] S. S. Mahboob, K. Swanson, J. A. Gonzalez, J. L. Shepherd, *J. Appl. Electrochem.* **46**, 539 (2016).
- [18] J. Ustarroz, J. A. Hammons, T. Altantzis, A. Hubin, S. Bals, H. Terryn, *J. Am. Chem. Soc.* **135**, 11550-11561 (2013).
- [19] D. Desai, D. E. Turney, B. Anantharaman, D. A. Steingart, S. Banerjee, *J. Phys. Chem. C* **118**, 8656-8666 (2014).
- [20] A. Zimmer, L. Broch, C. Boulanger, N. Stein, *Electrochim. Acta* **174**, 376-383 (2014).
- [21] L. Guo, A. Thompson, P. C. Searson, *Electrochim. Acta* **55**, 8416-8421 (2010).
- [22] T. Treeratanaphitak, M. D. Pritzker, N. M. Abukhdeir, *Electrochim. Acta* **121**, 407-414 (2014).
- [23] M. H. Mamme, E. A. M. Cherigui, O. Dolgikh, J. Ustarroz, H. Simillion, H. Terryn, J. Deconinck, *Electrochim. Acta* **197**, 307-317 (2016).
- [24] J. Xi, Q. Zhang, K. Park, Y. Sun, G. Cao, *Electrochim. Acta* **56**, 1960-1966 (2011).
- [25] A. M. Bakhshayesh, S. S. Azadfar, N. Bakhshayesh, *J. Mater. Sci. Mater. Electron.* **26**, 9808-9816 (2015).
- [26] X. Yanpeng, A. Taleb, P. Jegou, *J. Mater. Chem. A* **1**, 11580-11588 (2013).
- [27] J. Niu, X. Liu, K. Xia, L. Xu, Y. Xu, X. Fang, W. Lu, *Int. J. Electrochem. Sci.* **10**, 7331-7340 (2015).
- [28] D. N. Buckley, S. Ahmed, *Electrochem. Solid State Lett.* **6**, C33-C37 (2003).
- [29] A. Taleb, F. Mesguish, T. Onfroy, X. Yanpeng, *RSC Advances* **5**, 7007-7017 (2015).
- [30] G. L. M. K. S. Kahanda, X. Q. Zou, R. Farrell, and P. Z. Wong, *Phys. Rev. Lett.* **68**, 3741-3744 (1992).
- [31] J. M. Pastor, M. A. Rubio, *Phys. Rev. Lett.* **76**, 1848-1851 (1996).

- [32] M. C. Lafouresse, P. J. Heard, W. Schwarzacher, Phys. Rev. Lett. **98**, 236101:1-4 (2007).
- [33] J. R. de Bruyn, Phys. Rev. E **53**, R5561-R5564 (1996).
- [34] C. Léger, J. Elezgaray, F. Argoul, Phys. Rev. E **58**, 7700-7709 (1998).
- [35] M. A. Pasquale, S. L. Marchiano, P. L. Schilardi, R. C. Salvarezza, A. J. Arvia, Phys. Rev. E **65**, 041608:1-5 (2002).
- [36] J. Villain, J. Phys. I **1**, 19 (1991).
- [37] Z.-W. Lai and S. Das Sarma, Phys. Rev. Lett. **66**, 2348-2351 (1991).
- [38] J. Wang, Analytical Electrochemistry, 3rd ed. (Wiley, Hoboken, New Jersey, 2006).
- [39] F. D. A. Aarão Reis, Phys. Rev. E **81**, 041605:1-7 (2010).
- [40] S. Clarke and D. D. Vvedensky, J. Appl. Phys. **63**, 2272-2283 (1988).
- [41] J. W. Evans, P. A. Thiel, M. C. Bartelt, Surf. Sci. Rep. **61**, 1-128 (2006).
- [42] A.-L. Barabási, H. E. Stanley, Fractal Concepts in Surface Growth (Cambridge University Press, NY, 1995).
- [43] Y. Zhao, G.-C. Wang, and T.-M. Lu (Eds.), *Characterization of Amorphous and Crystalline Rough Surface: Principles and Applications*, in: Experimental Methods in the Physical Sciences vol. 37 (Academic Press, San Diego, CA, 2001).
- [44] D. Siniscalco, M. Edely, J. F. Bardeau, and N. Delorme, Langmuir **29**, 717 (2013).
- [45] F. D. A. Aarão Reis, J. Stat. Mech., P11020:1-19 (2015).
- [46] F. Family, T. Vicsek, J. Phys. A **18**, L75-L81 (1985).
- [47] J. J. Ramasco, J. M. López, M. A. Rodríguez, Phys. Rev. Lett. **84**, 2199-2202 (2000).
- [48] S. Huo and W. Schwarzacher, Phys. Rev. Lett. **86**, 256-259 (2001).
- [49] F. D. A. Aarão Reis, Phys. Rev. E **70**, 031607:1-8 (2004).
- [50] I. S. S. Carrasco, T. J. Oliveira, Phys. Rev. E **93**, 012801:1-10 (2016).
- [51] H. K. Janssen, Phys. Rev. Lett. **78**, 1082-1085 (1997).
- [52] D. di Caprio and F. D. A. Aarão Reis, Phys. Rev. E **92**, 012402:1-9 (2015).
- [53] T. A. de Assis and F. D. A. Aarão Reis, J. Stat. Mech., P06023:1-12 (2015).
- [54] T. A. de Assis and F. D. A. Aarão Reis, Phys. Rev. E **92**, 052405 (2015).
- [55] Y. Xu, X.-M. Ge, Y.-J. Tong, H.-L. Xie, T.-Q. Xiao, J.-Z. Jiang, Electrochem. Comm. **12**, 442-445 (2010).
- [56] Q. Zhang, T. P. Chou, B. Russo, S. A. Jenekhe, G. Cao, Adv. Fun. Mater **18**, 1654-1660 (2008).
- [57] Y. Cai, H. E. Wang, S. Z. Huang, M. F. Yuen, H. H. Cai, C. Wang, Y. Yu, Y. Li, W. J. Zhang, B. L. Su, Electrochimica Acta **210**, 206-214 (2016).
- [58] K. Zhang, X. Yang, Y. Wang, Y. Bing, L. Qiao, Z. Liang, S. Yu, Y. Zeng, W. Zheng, Sens. Actuator B-Chem. **243**, 465-474 (2017).
- [59] R. Mariappan, V. Ponnuswamy, P. Suresh, N. Ashok, P. Jayamurugan, A. Chandra Bose, Superlattices and Microstructures **71**, 238-249 (2014).
- [60] J. Yang, X. Li, S. L. Bai, R. X. Luo, A. F. Chen, Y. Lin, J. B. Zhang, Thin Solid Films **519**, 6241-6245 (2011).
- [61] Y. Y. Chun, D. H. Peck, C. S. Kim, D. R. Shin, J. New Mater. Electrochem. Syst., **4**, 31-35 (2001).
- [62] H. Li, K. K. Tung, D. R. Paul, B. D. Freeman, Polymer **52**, 27772 (2011).
- [63] W. W. Mullins, J. Appl. Phys. **28**, 333-339 (1957).
- [64] A. Sánchez, M. J. Bernal, J. M. Riveiro, Phys. Rev. E **50**, R2427-R2431 (1994).
- [65] M. Castro, R. Cuerno, A. Sánchez, F. Domínguez-Adame, Phys. Rev. E **57**, R2491-R2494 (1998).
- [66] D. A. Cogswell, Phys. Rev. E **92**, 011301(R) (2015).